Journal of Power Sources 248 (2014) 894–899

Contents lists available at ScienceDirect

Journal of Power Sources

journal homepage: www.elsevier.com/locate/jpowsour

Enhanced oxygen reducibility of $0.5Li_2MnO_3 \cdot 0.5LiNi_{1/3}Co_{1/3}Mn_{1/3}O_2$ cathode material with mild acid treatment

Guofeng Xu [a], Jianling Li [a,*], Qingrui Xue [a], Xianping Ren [a], Gang Yan [a], Xindong Wang [a], Feiyu Kang [b]

[a] State Key Laboratory of Advanced Metallurgy, University of Science and Technology Beijing, No. 30 College Road, Haidian District, Beijing 100083, China
[b] Lab of Advanced Materials, Department of Materials Science and Engineering, Tsinghua University, Beijing 100084, China

HIGHLIGHTS

- The H^+/Li^+ exchange reaction is triggered by a mild acid solution.
- In-situ CV method is adopted to explain the mechanism of acid treatment.
- The treated electrode shows elevated initial cycle efficiency and rate performance.
- The elevated capability is attributed to the enhanced oxygen reducibility.

ARTICLE INFO

Article history:
Received 22 July 2013
Received in revised form
26 September 2013
Accepted 1 October 2013
Available online 15 October 2013

Keywords:
Acid treatment
Hydrogen/lithium ion-exchange
Oxygen reducibility
Solid solution material
Lithium ion battery

ABSTRACT

Solid solution cathode material $0.5Li_2MnO_3 \cdot 0.5LiNi_{1/3}Co_{1/3}Mn_{1/3}O_2$ has been synthesized by a co-precipitation method and a mild acid was adopted to give rise to the H^+/Li^+ exchange reaction. The inductively coupled plasma-atomic emission spectrometry (ICP-AES) and atomic absorption spectroscopy (AAS) data show that the H^+/Li^+ exchange reaction actually occurs and the chemical composition is $H_{0.06}Li_{1.15}Ni_{0.13}Co_{0.14}Mn_{0.55}O_{2.03}$ after the material was treated. The X-ray powder diffraction patterns indicates that the structure doesn't change through the H^+/Li^+ exchange reaction and remains the hexagonal α-$NaFeO_2$ layered structure with space group of R-3m. The field-emission scanning electron microscope (SEM) and transmission electron microscope (TEM) images show that there are traces of erosion on the surface of the H^+/Li^+ exchanged sample. The initial charge–discharge curve measured at 0.05C (12.5 mA g^{-1}) demonstrates that the H^+/Li^+ exchanged electrode delivers a capacity of up to 314.0 mAh g^{-1} and coulombic increased initial efficiency. Cycle voltammetry (CV) measurement confirms this is attributed to the improvement of the reduction catalytic activity of oxygen released during the initial charging. The processed electrode also displays improved rate performance.

1. Introduction

Solid solution oxides $xLi_2MnO_3 \cdot (1-x)LiMO_2$ (M = Mn, Ni, Co, etc.), alternatively as a layer type $Li_{1+x}M_{1-x}O_2$ (represented by LMO in this article), are of great potential as cathode materials for lithium ion batteries. The Li_2MnO_3 and $LiMO_2$ components are structurally integrated to form highly complex atomic arrangements in which Li_2MnO_3 and Li_2MnO_3-like domains exist with short-range order within a layered $LiMO_2$ matrix [1]. This serial of materials delivers an anomalously high discharge capacity of more than 270 mAh g^{-1} at a low rate (0.05C) between 2.0 V and 4.8 V [2–5], which made them appealing in recent years. However, the solid solution materials undergo an irreversible loss of oxygen from the lattice and suffer from a huge irreversible capacity loss of 40–100 mAh g^{-1} in the first cycle [6,7].

As is proved that the initial irreversible capacity of these materials is much related to the 4.5 V plateau during the initial charging. Up to now, oxygen release of the initial charging process when the electrode is charged to the typically 4.5 V plateau has been confirmed [7–11]. However, whether the released oxygen is reduced in the following charging process is questioned. In consideration of the theoretical capacity of oxygen reaches 837 mAh g^{-1} assuming that only one electron is transmitted for every oxygen molecule, it matters even if the small amount of oxygen molecule is reduced. A recent research by Yabuuchi et al. [10] proved that the oxygen molecules indeed participate in the

* Corresponding author. Tel./fax: +86 10 6233 2651.
E-mail address: lijianling@ustb.edu.cn (J. Li).

0378-7753/$ – see front matter © 2013 Elsevier B.V. All rights reserved.
http://dx.doi.org/10.1016/j.jpowsour.2013.10.002

electrochemical redox reaction making the practical capacity higher than the theoretical capacity and that the redox reaction is partly reversible. Hence, the behavior of the solid solution cathode material can be considered as the complex processes for both Li-ion cell and Li-air cell. And how to improve the reducibility of the oxygen or oxygen-containing species will be an important issue for the optimization of the high-capacity solid solution positive electrode materials.

Generally, acid treatment is intended to improve the initial coulombic efficiency. There are two main processes during acid treatment: the first step is H^+/Li^+ exchange reaction and the following step is the deintercalation of Li_2O or/and H_2O from the structure, and that the deintercalated lithium mainly comes from the Li_2MnO_3 component. In addition, the H^+/Li^+ exchange reaction occurs at elevated temperature (55 °C) based on the study on pure phase Li_2MnO_3 [10]. And the cells show anomalous high capacity and good cycling stability tested in 50 °C [12]. Thus, a hypothesis is proposed that the H^+/Li^+ exchange reaction is conductive to the oxygen reducing ability and accordingly, contributes to the anomalous capacity and cycling stability.

However, the condition of electrode surface deteriorates rapidly during circulation when the samples are treated with high concentration acid [13]. What's more, there has been no explanation for the mechanism of elevated performance with acid treatment. In this work, chemical delithiation method was adopted to trigger the H^+/Li^+ exchange reaction. An acid solution with low concentration was used to enhance the oxygen reducing ability as well as maintain the inner structure at the same time. In-situ CV method was introduced to explain the mechanism of acid treatment. The effects of physical and chemical properties of mild acid treatment are reported in the following.

2. Experimental

The solid solution cathode material $0.5Li_2MnO_3 \cdot 0.5LiNi_{1/3}Co_{1/3}Mn_{1/3}O_2$ was synthesized by a fast co-precipitation method using sulfates as the sources [14].

The lithium extraction from Li_2MnO_3 component consuming equivalent H^+ in the solution via the mechanism of a H^+/Li^+ ion exchange reaction when $[H^+]_l/[Li^+]_s \leq 0.15$ according to Tang's research [13]. Therefore, in our research the H^+/Li^+ exchanged samples were obtained through leaching pristine material with 0.01 mol L^{-1} HNO_3 ($[H^+]_l/[Li^+]_s = 0.1$) with continuous stirring for 2 h at room temperature. The mild acid not only supplied the H^+ for H^+/Li^+ exchange reaction but also minimized the damage on the surface and structure of the cathode material. The leached material was filtered, washed, and oven-dried at 100 °C for 24 h and the filtrate was also collected. The pH of the solution was monitored during the above process by an acidometer (PHS-3C, Rex, Shanghai). The amount of the leached Li^+ in the filtrate was measured with atomic absorption spectroscopy (AAS, AA-6800, Shimadzu, Japan). Inductively coupled plasma-atomic emission spectrometry (ICP-AES, OPTIMA 7000DV, Perkin–Elmer Co., Ltd., America) analyses were conducted on the parent material and on the processed samples to monitor the variances of the relative amounts of Li, Mn, Ni, and Co in the samples.

Table 1
Relative amounts of Li, Ni, Co, Mn in the pristine material and in an acid-treated product (ICP data).

	Li	Ni	Co	Mn	H
Theoretical value	1.20	0.13	0.13	0.54	–
Pristine samples	1.22	0.13	0.14	0.55	–
Treated samples	1.15	0.13	0.14	0.55	0.06

The structures and morphologies of the pristine and treated samples were analyzed by X-ray powder diffraction (XRD, Rigaku RINT2400 with Cu Kα radiation, $\lambda = 1.54056$ Å), field-emission scanning electron microscopy (FESEM, Zeiss SuprATM 55 microscope) and transmission electron microscopy (TEM, JEOL JEM-2100). The electrochemical properties were studied by using CR2032 coin cells and three-electrode system. The work electrodes were fabricated by a mixture of active material, acetylene black and polyvinylidene fluoride (PVDF) in the weight ratios of 80:10:10. The as-prepared slurry was coated on Al foil for coin cells and on the foam nickel (1 cm × 1 cm) for three-electrode system respectively. The prepared electrodes were dried at 120 °C overnight under vacuum prior to use. The electrolyte was 1 mol L^{-1} $LiPF_6$ in EC/DMC (volume ratio 1:1) and the porous polypropylene film was placed between cathode and anode. The initial charge–discharge test was studied at 0.05C (12.5 mA g^{-1}) and the cycling performance was carried out at 0.2C (50.0 mA g^{-1}) in the voltage range of 2.0–4.8 V. For the rate tests, lithium cells were charged to 4.8 V at 0.1C (25.0 mA g^{-1}) and were discharged to 2.0 V at different rates successively.

The oxygen reductive capabilities of the electrodes before and after charge were measured by in-situ cyclic voltammetry in VMP2 electrochemical workstation (Princeton Applied Research, USA), in which the reference electrode was saturated calomel electrode and

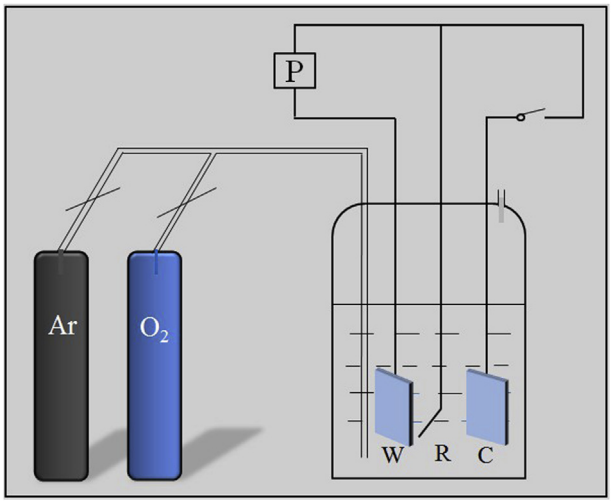

Fig. 1. Schematic of the installment of in-situ cyclic voltammetry.

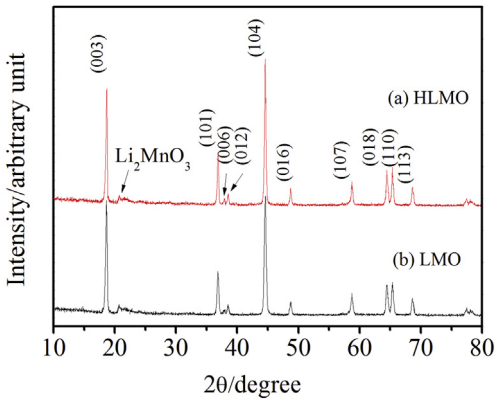

Fig. 2. XRD patterns of the pristine sample (LMO) and H^+/Li^+ exchanged sample (HLMO).

Table 2
Refined unit cell parameters of the parental and H^+/Li^+ exchanged samples.

Compound	*a*	*c*	*V*	*c*/*a*
$Li_{1.22}Ni_{0.13}Co_{0.14}Mn_{0.55}O_{2.04}$ (LMO)	2.85582	14.25632	100.69	4.992
$H_{0.06}Li_{1.15}Ni_{0.13}Co_{0.14}Mn_{0.55}O_{2.03}$ (HLMO)	2.85521	14.24184	100.55	4.988

the counter electrode was Li sheet. The schematic of the installment is shown in Fig. 1. All tests were taken at room temperature.

3. Results and discussion

3.1. Composition determination

Table 1 shows the relative amounts of each component measured by the ICP-AES. The chemical composition of untreated sample was $Li_{1.22}Ni_{0.13}Co_{0.14}Mn_{0.55}O_{2.04}$ (represented by LMO in this article) determined by ICP data. Moreover, the consistency of Mn:Ni:Co ratio between pristine and treated samples suggests that minimal dissolution of the transition metal ions had occurred during the acid-leaching process. However, the lithium content was significantly reduced by acid treatment as expected. This proved that Li^+ had deintercalated from the structure, which was supported by the atomic absorption spectroscopy (AAS) measurement for the collected filtrate. The amount of Li^+ in the filtrate measured by AAS was highly consistent with the lithium loss after leaching indicated by ICP data. The variation of the pH of the acid solution was measured by the acidometer. Before leaching the pH value was 1.98 and the value reached 6.55 after two hour's leaching. The change of pH value indicated the H^+ ions embedded into the structure of the material from the acid solution. In addition, the H^+ loss calculated through the change of pH value in the acid solution was close with the amount of the lithium in the filtrate.

It suggests that the H^+ in the solution replaced equimolar Li^+ in the material by the mechanism of H^+/Li^+ exchange reaction and the exact chemical composition of the leaching products can be determined to be $H_{0.06}Li_{1.15}Ni_{0.13}Co_{0.14}Mn_{0.55}O_{2.03}$ (represented by HLMO in this article) through both the AAS measurement and ICP-AES measurement.

3.2. Structure and morphology

The powder XRD patterns of the parent compound and the acid-treated product are shown in Fig. 2. The main peaks of the patterns can be indexed to the space group of R3-*m* layered symmetry based on the hexagonal α-$NaFeO_2$ structure. The reflection at ~21°, which is the characteristic of the integrated monoclinic Li_2MnO_3-like component (C2/*m*) due to the Li cation ordering in the metal layer. The peak intensity at 21° for the acid treated products reduces slightly which is consistent with lithium extraction from the transition metal layers of the Li_2MnO_3 component. The lattice parameter refinements listed in Table 2 are based on the pseudo rhombohedral symmetry, R3-*m*. It is evident that the values of *c* and *V* decrease after acid leaching which can be induced by the slight contraction of the oxygen planes during the H^+/Li^+ exchange reaction. The H^+/Li^+ exchange reaction maintains the structure and a single phase yields during treatment.

The SEM and TEM images in Fig. 3 show that the particle size of synthesized products is in range of 100–200 nm and the acid leaching process did not modify the particle size. The surface of H^+/Li^+ exchanged sample is smoother than the pristine one. Fig. 3(c) displays a disconnected amorphous layer on the surface of particle while there is no amorphous layer formed in Fig. 3(d). In addition, a thin amorphous layer was also found on the Li-excess oxide particle surface by Hong et al. [15]. The amorphous layer may have contained Li_2O and $LiCO_3$, which is available for Li-ion diffusion but unfavorable for electron conduction. It indicates that the H^+/Li^+ exchange reaction mainly occur at the surface of particle and is beneficial to the electron conduction.

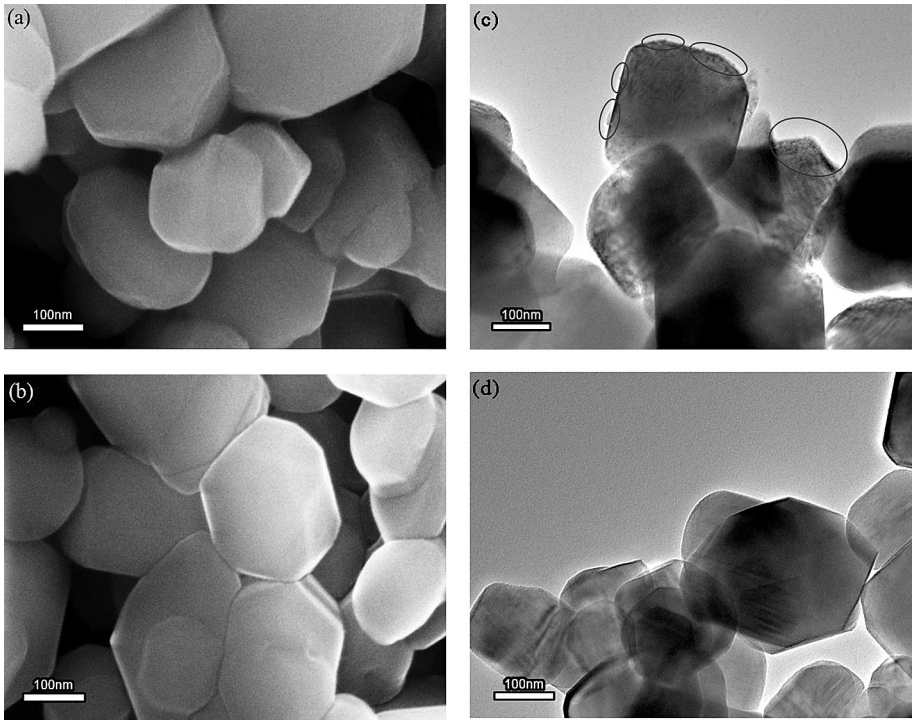

Fig. 3. SEM images of pristine (a) and H^+/Li^+ exchanged (b) samples. TEM images of pristine (c) and H^+/Li^+ exchanged (d) samples.

3.3. Electrochemical analysis

The theoretical capacity is calculated to be 314 mAh g^{-1} based on one electron redox per formula unit of $Li_{1.2}Ni_{0.13}Co_{0.13}Mn_{0.54}O_2$. As we know that the apparent capacity is limited by the transferred electrons of transition metals in the oxidation/reduction process. The rechargeable capacity is calculated to be 290 mAh g^{-1} based on the solid-state redox of each transition metal ($Co^{3+/4+}$, $Ni^{2+/3+/4+}$, $Mn^{3+/4+}$), corresponding to 0.92 mol lithium reversible deintercalation/intercalation. Fig. 4(a) gives the initial charge–discharge curves of samples before and after delithiation at a low current density of 12.5 mA g^{-1}. For the charge process, both electrodes deliver the capacity exceeding 340 mAh g^{-1} and approaching to 1.1 mol lithium deintercalation. The discharge capacity of untreated material electrode is 301.4 mAh g^{-1} (0.96 mol lithium intercalation) while the H^+ contained electrode shows 314.0 mAh g^{-1} capacity (1.0 mol lithium intercalation). These capacity data indicate that the H^+/Li^+ exchange reaction occurred in the acid treatment process improve the initial coulombic efficiency from 82.4% to 89.7%. Moreover, both electrodes, especially to H^+ contained electrode, deliver practical capacity exceeding the theoretical capacity 290 mAh g^{-1}. This means that there must be some other charge–discharge mechanisms besides the traditional electronic transferred behaviors to balance the lithium intercalation/deintercalation at least for the initial cycle. At present, it is confirmed that the balance behavior for initial charge process is attributed to the lattice oxygen turning into the free oxygen molecules. However, the balance behavior for discharge processes (at least for the first cycle) is also in dispute. It is most likely that the oxygen molecules participate in the reduction process because the oxygen can be reduced on the electrode surface in the presence of catalyst behaving the same as the Li–O_2 cells considering that the manganese oxides also can be used as the catalyst for Li–O_2 cells [16]. The specific behavior of oxygen during initial discharge process and how the H^+/Li^+ exchange reaction affects on it are discussed in detail in following parts.

The dQ/dV plots for first cycle are shown in Fig. 4(b) and there are two evident oxidation peaks at 4.0 V and 4.5 V respectively for both untreated electrode and treated electrode. The peak at 4.0 V is attributed to the process of lithium deintercalation from the $Li(Mn_{1/3}Co_{1/3}Ni_{1/3})O_2$ component accompanying with the oxidation of transition metals and another peak at 4.5 V is corresponding to the process of further lithium deintercalation and oxygen release from the Li_2MnO_3 component. Moreover, three reduction peaks are evident on discharge, but it is difficult to differentiate the reduction processes of the individual Mn, Ni, and Co ions, it is believed from theoretical analysis that the different peaks may be associated with the occupation of different sites of lithium. The peak at 2.64 V for the H^+-free electrode and the peak at 2.73 V for the H^+-contained electrode and the ~0.1 V shift between these two peaks are different from the common ternary materials such as $LiNi_{1/3}Co_{1/3}Mn_{1/3}O_2$ [17]. Naoaki Yabuuchi et al. [10] consider the peaks are much related to the reduction of oxygen or it's species on the electrode surface. Another basis for supporting the oxygen

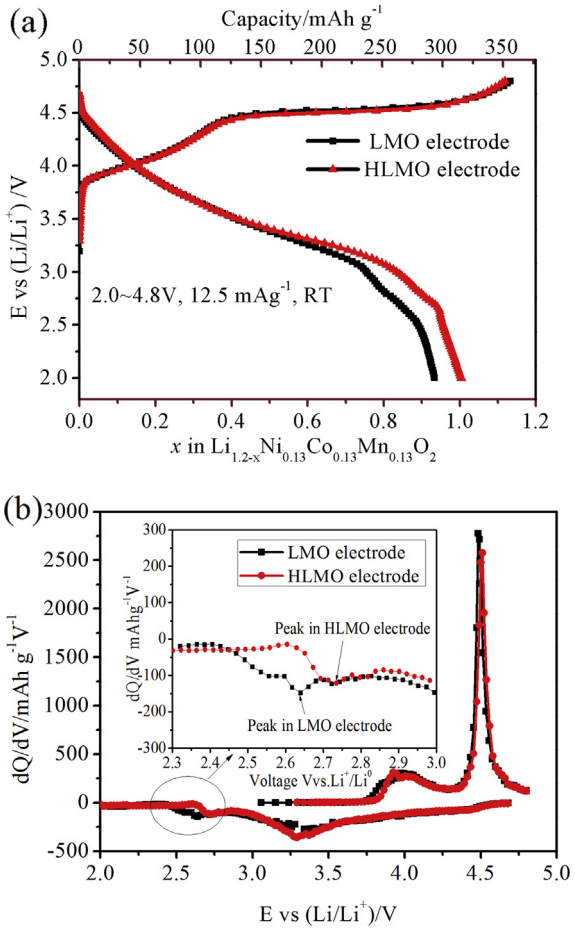

Fig. 4. (a) Initial charge and discharge profiles of lithium half cells with $Li_{1.22}Ni_{0.13}Co_{0.14}Mn_{0.55}O_{2.04}$ (LMO) and $H_{0.06}Li_{1.15}Ni_{0.13}Co_{0.14}Mn_{0.55}O_{2.03}$ (HLMO) electrodes. (b) The differential capacity (dQ/dV) plots corresponding to initial charge and discharge profiles.

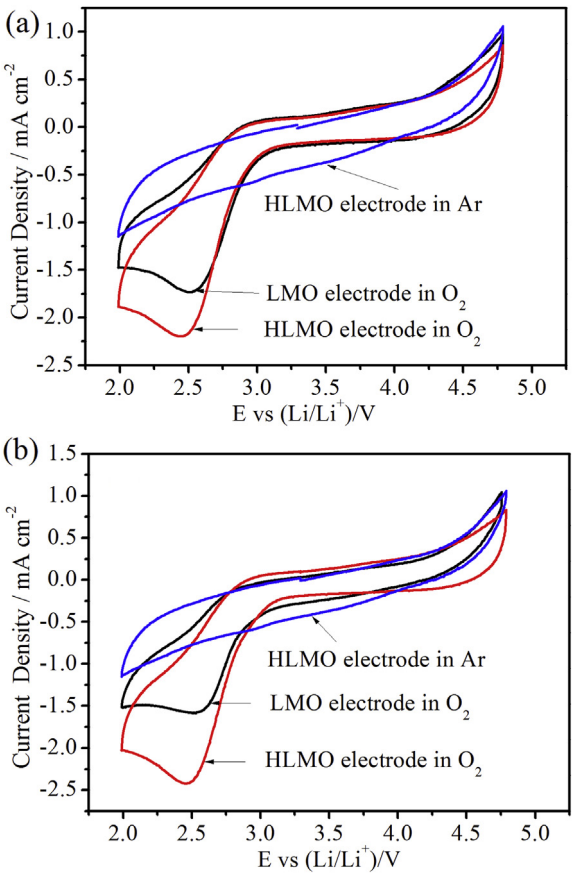

Fig. 5. In-situ cyclic voltammetry vs. standard SCE for samples LMO and HLMO at a scan rate of 50 mV s^{-1}. (a) Before charging and (b) after initial charging to 4.8 V.

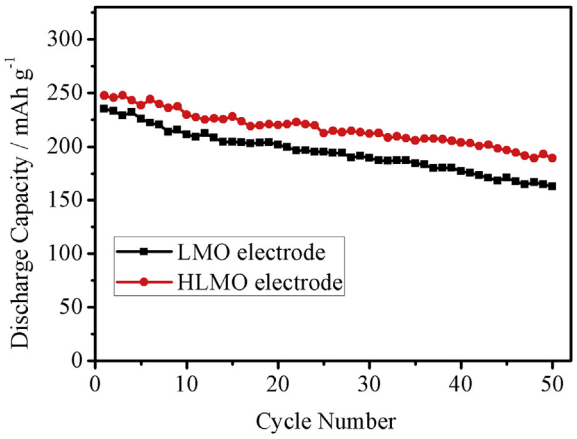

Fig. 6. Comparison of cycle abilities of LMO and HLMO with a current density of 50 mA g^{-1}.

reduction theory is that the peaks also can be seen in Li-air system (~2.7 V vs. Li^+/Li^0) where Li_2MnO_3 was used as oxygen reduction catalyst [18]. Thus, the solid solution cathode not only acts as a host for lithium but also acts as a reduction catalyst for oxygen molecules released during initial charging. At the same time, the H^+/Li^+ exchanged reaction strengthens the oxygen reduction ability and makes the reduction potential of the oxygen higher than the H^+-free electrode.

For further research, in-situ CV test was carried out in the electrolyte consisting of 1 M $LiPF_6$ in a mixture of EC: DMC (1:1) with the scan rate of 50 mV s^{-1}. For the H^+/Li^+ exchanged electrode, the cyclic voltammetry tests were firstly carried out in Ar and O_2 atmosphere successively. And after charging to 4.8 V in Ar atmosphere, the electrode was tested in Ar and O_2 successively as well as the electrode before charging. And the pristine electrode was tested in O_2 atmosphere before and after charging successively. The plots are shown in Fig. 5.

Fig. 5 suggests that there are no evident peaks before charging for HLMO electrode tested in Ar atmosphere in whole voltage range as well as the electrode after charging. However, when tested in O_2 the reduction peaks observed at ~2.5 V which are very close to the peaks in dQ/dV plots (Fig. 4(b)) are evident for both LMO electrode and HLMO electrode before and after charging. Based on the facts above, it can be concluded that the ~2.5 V peaks shown in Figs. 4(b) and 5 are the characteristics of oxygen

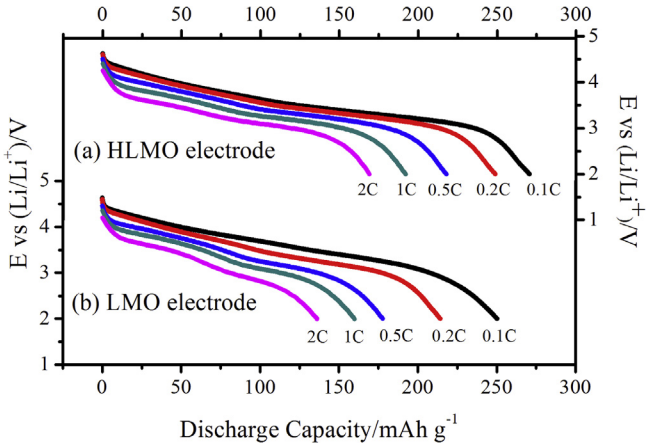

Fig. 7. Rate capabilities for (a) HLMO electrode and (b) LMO electrodes measured galvanostatically at various discharge rates.

reduction, as a result, the practical capacity exceeds the theoretical capacity. On one hand, the electrodes tested in O_2 after charging shown in Fig. 5(b) have higher oxygen reduction currents than the electrodes before charging. The phenomenon may be ascribed to the formation of oxygen vacancies after initial charging. On the other hand, the H^+-contained electrode have higher O_2 reduction currents than the pristine one, especially to the electrode after charging which indicate the HLMO sample has better catalytic ability for O_2.

The 2.5 V peaks in CV plots and ~2.7 V peaks in dQ/dV plot are identified as the characteristics of oxygen reduction which is the reason of practical capacity exceeding the theoretical capacity for the first cycle. And the H^+/Li^+ exchanged reaction improves the catalytic ability of oxygen which explains why the H^+-contained electrode delivers higher capacity than the H^+-free electrode.

As is shown in Fig. 6, the HLMO electrode shows slightly better cycling ability than the LMO electrode. It is because that we used an acid solution with lower concentration to realize the H^+/Li^+ exchanged reaction, as a result, the destruction to inner structure of the material was controlled to a lower level and the oxygen reduction was ensured at the same time.

Rate capacities of LMO and HLMO electrodes are shown in Fig. 7. The HLMO electrode delivers higher capacity than the LMO electrode at various rates, particularly, the capacity of the HLMO electrode reaches to 166.8 mAh g^{-1} at 2C while only 138.8 mAh g^{-1} is obtained by LMO electrode. The improvement of the rate performance mainly benefits from the reduced irreversible capacity of first cycle caused by enhanced oxygen reducibility. The formation of expedite lithium channels originated from the H^+/Li^+ exchanged reaction promotes the rate capability at the same time.

4. Conclusions

Solid solution cathode material $0.5Li_2MnO_3 \cdot 0.5LiNi_{0.33}Co_{0.13}Mn_{0.54}O_2$ (represented by LMO as a layer type) was synthesized by a co-precipitation method and a mild acid solution was utilized to make the H^+/Li^+ exchange happen. The ICP-AES and AAS data show that the H^+/Li^+ exchange reaction indeed happened and the chemical composition of the products was determined to be $H_{0.06}Li_{1.15}Ni_{0.13}Co_{0.14}Mn_{0.55}O_{2.03}$ (represented by HLMO). The XRD patterns showed that the inner structure was not changed through the H^+/Li^+ exchange reaction and remained the space group of R3-m layered symmetry based on the hexagonal α-$NaFeO_2$ structure. SEM images indicated that traces of erosion exist at the surface of the H^+/Li^+ exchanged sample. The initial charge–discharge measured at 0.05C showed that the H^+/Li^+ exchanged electrode delivered capacity of 314.0 mAh g^{-1}. The treated electrode displays elevated rate performance and the treatment improves the initial cycle efficiency from 82.4% to 89.7%. In-situ CV measurement proclaimed this was attributed to the improvement of the reductive catalytic activity of oxygen released during initial charge process. Thus, some techniques aimed to enhance the reductive catalytic activity of oxygen of Li–O_2 cells and fuel cells can be further employed in the Lithium-ion cells with solid solution cathode materials.

Acknowledgments

This work is financially supported by the National Natural Science Foundation of China (no.51172023), the National Basic Research Program of China (973 Program, 2013CB934002), the National High Technology Research and Development Program of China (863 Program, 2012AA110302), and the National Natural Science Foundation of China (no. 51372021).

References

[1] S.H. Kang, C.S. Johnson, J.T. Vaughey, K. Amine, M.M. Thackeray, J. Electrochem. Soc. 153 (2006) A1186–A1192.
[2] Young Sik Hong, Yong Joon Park, Kwang Sun Ryu, Soon Ho Chang, Min Gyu Kim, J. Mater. Chem. 14 (2004) 1424–1429.
[3] D.K. Lee, S.H. Park, K. Amine, H.J. Bang, J. Parakash, Y.K. Sun, J. Power Sources 162 (2006) 1346–1350.
[4] Min Gyu Kim, Minki Jo, Young Sik Hong, Jaephil Cho, Chem. Commun. 2 (2009) 218–220.
[5] J. Li, R. Klöpsch, M.C. Stan, S. Nowak, M. Kunze, M. Winter, S. Passerini, J. Power Sources 196 (2011) 4821–4825.
[6] Z.H. Lu, J.R. Dahn, J. Electrochem. Soc. 149 (2002) A815–A822.
[7] A.R. Armstrong, M. Holzapfel, P. Novak, C.S. Johnson, S. Kang, M.M. Thackeray, P.G. Bruce, J. Am. Chem. Soc. 128 (2006) 8694–8698.
[8] Z. Lu, J.R. Dahn, J. Electrochem. Soc. 149 (2002) A778–A791.
[9] J.S. Kim, C.S. Johnson, J.T. Vaughey, M.M. Thackeray, S.A. Hackney, W. Yoon, C.P. Grey, Chem. Mater. 16 (2004) 1996–2006.
[10] Naoaki Yabuuchi, Kazuhiro Yoshii, Seung Taek Myung, Izumi Nakai, Shinichi Komaba, J. Am. Chem. Soc. 133 (2011) 4404–4419.
[11] Chaolun Gan, Hui Zhan, Xiaohong Hu, Yunhong Zhou, Electrochem. Commun. 7 (2005) 1318–1322.
[12] Christopher S. Johnson, Naichao Li, Christina Lefief, Michael M. Thackeray, Electrochem. Commun. 9 (2007) 787–795.
[13] Weiping Tang, Hirofumi Kanoh, Xiaojing Yang, Kenta Ooi, Chem. Mater. 12 (2000) 3271–3279.
[14] Yu Chen, Guofeng Xu, Jianling Li, Yakun Zhang, Zhong Chen, Feiyu Kang, Electrochim. Acta 87 (2013) 686–692.
[15] Jihyun Hong, Hee Dae Lim, Minah Lee, Sung Wook Kim, Haegyeom Kim, Song Taek Oh, Geun Chang Chung, Kisuk Kang, Chem. Mater. 24 (2012) 2692–2697.
[16] Hun Gi Jung, Jusef Hassoun, Jin-Bum Park, Yang Kook Sun, Bruno Scrosati, Nat. Chem. 4 (2012) 579–585.
[17] Xiao Jian Guo, Yi Xiao Li, Min Zheng, Jian Ming Zheng, Jie Li, Zheng Liang Gong, Yong Yang, J. Power Sources 184 (2008) 414–419.
[18] J. Katana, Shaun Alia, Arthur Dobley, B. Vincent Mark, Crisostomo, Steven L. Suib, Chem. Mater. 19 (2007) 229–234.